Role of Renner Teller and Spin−Orbit Interaction in the Dynamics of the $O(^3P) + C_3H_5I$ Reaction

J. J. Wang, D. J. Smith, and R. Grice*

Chemistry Department, University of Manchester, Manchester M13 9PL, U.K.

Received: July 22, 1996; In Final Form: March 12, 1997[⊗]

Reactive scattering of $O(^3P)$ atoms with C_3H_5I molecules has been studied at initial translational energies $E \sim 46$ and 16 kJ mol^{-1} using a supersonic beam of O atoms seeded in He and Ne buffer gas generated from a microwave discharge source. Strongly backward peaked angular distributions of IO product scattering are observed at both initial translational energies with the peaking becoming sharper at higher energy. The product translational energy distributions are pitched at higher energy for the backward scattering and shift progressively toward lower energy as the IO scattering moves round into the forward direction. Backward scattering with high product translational energy is attributed to direct reaction in small impact parameter collisions $b \leq 2.5$ Å over the triplet potential energy surface. Scattering with low product translational energy which becomes perceptible in the forward direction is attributed to intersystem crossing to the underlying singlet potential energy surface forming a bound OIC_3H_5 intermediate complex. Direct reaction over the $^3A''$ potential energy surface plays a more significant role for the exoergic allyl iodide reaction than in the nearly thermoneutral reactions of alkyl iodide molecules, where intersystem crossing to the $^1A'$ potential energy surface is the predominant reaction mechanism. The dynamical basis for this difference in mechanism is discussed in terms of the topography of the potential energy surfaces involved.

Introduction

Recent measurements of the reactive scattering of ground state $O(^3P)$ atoms with alkyl iodide molecules[1,2] have shown evidence for intersystem crossing from the initial triplet potential energy surface to the underlying singlet potential energy surface, resulting in the formation of both IO and HOI reaction products.[3−5] The IO product may be formed either by direct reaction over the triplet potential energy surface or by simple bond fission of the OIR singlet intermediate, while HOI product is formed by dissociation of the singlet OIR intermediate via a five-membered ring transition state. The probability of intersystem crossing depends upon the initial translational energy, while the relative yield of HOI product depends upon the number of terminal CH_3 groups of the alkyl radical R. However, the precise location and mode of action of the seam of intersection between the triplet and singlet potential energy surfaces are not fully defined by these experimental results. In order to resolve the mechanism of intersystem crossing in the reactions of $O(^3P)$ atoms with hydrocarbon iodide molecules more clearly, the more exoergic reaction of allyl iodide molecules studied previously[6] is reported in full here:

$$O(^3P) + C_3H_5I \rightarrow IO(^2\Pi_{3/2}) + C_3H_5 \quad (1a)$$

$$\rightarrow IO(^2\Pi_{1/2}) + C_3H_5 \quad (1b)$$

Experimental Section

The apparatus was the same as that employed in previous preliminary experiments,[6] except that the quadrupole mass spectrometer detector has been rebuilt to gain improved resolution of the IO^+ mass peak while maintaining high detection sensitivity. Supersonic beams of $O(^3P)$ atoms seeded in He and Ne buffer gases were produced from a high-pressure microwave discharge source.[7] The allyl iodide beam issued from a glass nozzle of diameter ∼0.25 mm using a stagnation pressure of ∼50 mbar maintained by a reservoir at ∼0 °C. The velocity distributions of the O atom beams were measured by a beam monitor mass spectrometer and the C_3H_5I beam was measured by the rotatable mass spectrometer detector using pseudorandom cross-correlation time-of-flight analysis,[8] yielding the peak velocities v_{pk}, full widths at half-maximum intensity v_{wd}, and Mach numbers M listed in Table 1. The time-of-flight analysis employed a channel width of ∼10 μs in measuring the O atom beam velocity over a path length of 53 cm and the IO scattering and the C_3H_5I beam velocity over a path length of 13 cm.

TABLE 1: Beam Velocity Distributions, Peak Velocity v_{pk}, Full Width at Half-Maximum Intensity v_{wd}, and Mach Number M

beam	v_{pk}/m s^{-1}	v_{wd}/m s^{-1}	M
O (He)	2460	665	7
O (Ne)	1375	425	6
C_3H_5I	490	275	3

Results

Angular distribution measurements of IO reactive scattering measured on the 143 mass peak yield ∼33 and ∼16 counts s^{-1} against backgrounds of ∼12 and ∼7 counts s^{-1} for O atoms seeded in He and Ne buffer gases. The laboratory angular distributions of IO scattering in Figures 1 and 2 both peak close to the C_3H_5I beam. In order to check for distortion of the signal measured at the 143 mass peak arising from elastic scattering of cross-beam molecules in the vicinity of the C_3H_5I beam, measurements were also made using a dilute mixture of Ne in He buffer gas in the microwave discharge source. The resulting corrections amounted to only ∼2% for angles adjacent to the C_3H_5I beam. The laboratory velocity distributions of IO scattering in Figures 3 and 4 were measured using integration times of ∼2000−4000 s to gain signal-to-noise ratios of ∼10 at the peaks of the distributions. Kinematic analysis of these data has been undertaken using the forward convolution method[9]

[⊗] Abstract published in *Advance ACS Abstracts,* April 15, 1997.

S1089-5639(96)02203-7 CCC: $14.00

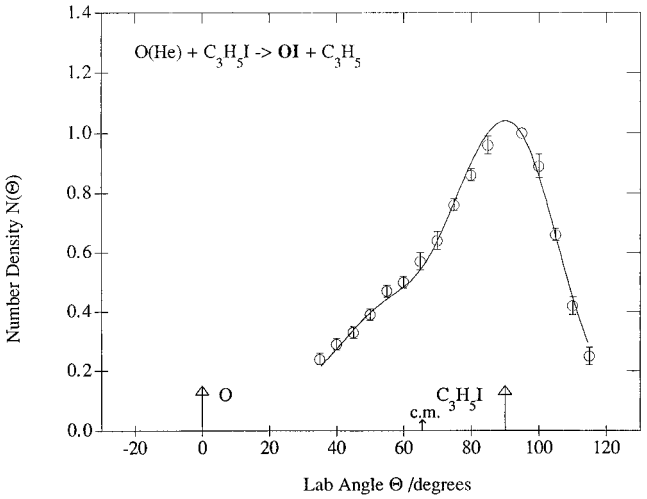

Figure 1. Laboratory angular distribution (number density) of IO reactive scattering measured at $m/e = 143$ from O + C_3H_5I at initial translational energy $E \sim 46$ kJ mol^{-1}. Solid line shows the fit of the kinematic analysis. The laboratory centroid is located at $\Theta_{cm} = 65°$.

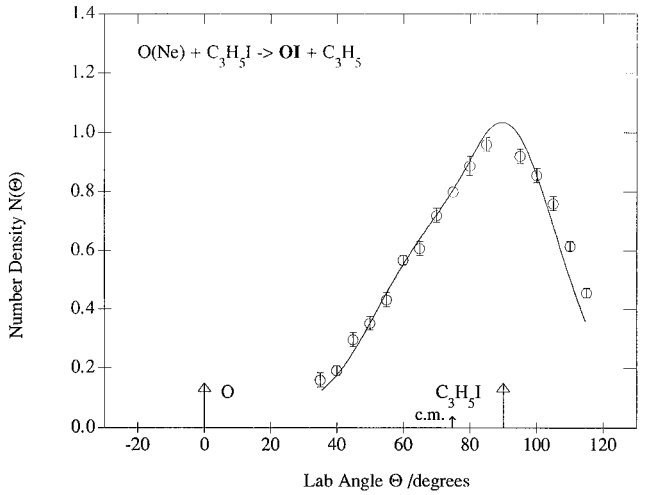

Figure 2. Laboratory angular distribution (number density) of IO reactive scattering from O + C_3H_5I at initial translational $E \sim 16$ kJ mol^{-1}. The laboratory centroid is located at $\Theta_{cm} = 75°$.

with the differential cross section expressed as a product of an angular function $T(\theta)$ and a velocity function $U(u,\theta)$ parametrically dependent on center-of-mass scattering angle

$$I_{cm}(\theta,u) = T(\theta)\, U(u,\theta) \qquad (2)$$

The center-of-mass angular distributions for IO product in Figures 5 and 6 are both backward peaked with the peaking becoming sharper at higher initial translational energy. The angular distribution has a Gaussian form in the backward hemisphere for reaction at lower initial translational energy $E \sim 16$ kJ mol^{-1}, but this is replaced by a Halpern−Strutinski form[10] for reaction at higher initial translational energy E ~ 46 kJ mol^{-1}. The product translational energy distributions $P(E')$ both dispose a substantial fraction $f' \sim 0.3$ of the total available energy into product translation. The product translational energy distributions both vary strongly with scattering angle being pitched at higher energy for the backward scattering and declining to lower energy as the IO scattering moves into the forward direction. The forward convolved fits to the experimental data are shown by solid curves in Figures 1−4. The peak E'_{pk} and average E'_{av} product translational energies are listed in Table 2, together with the initial translational energies E and the reaction exoergicities ΔD_0 estimated from the bond energies

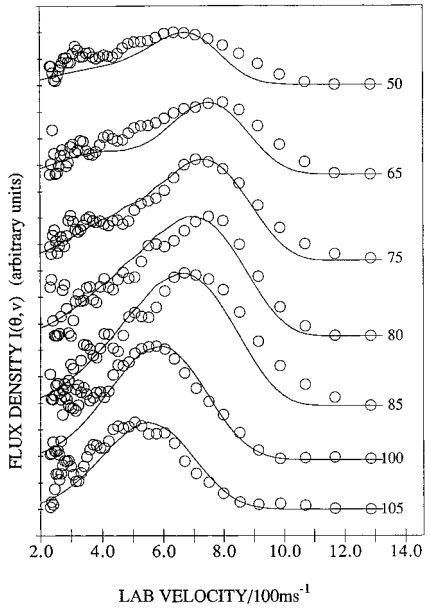

Figure 3. Laboratory velocity distributions (flux density) of reactively scattered IO measured at $m/e = 143$ from O + C_3H_5I at an initial translational energy $E \sim 46$ kJ mol^{-1}. Solid line shows the fit of the kinematic analysis. The relative errors at the peaks of the distributions are ∼0.1, increasing to ∼1 at the highest and lowest velocities.

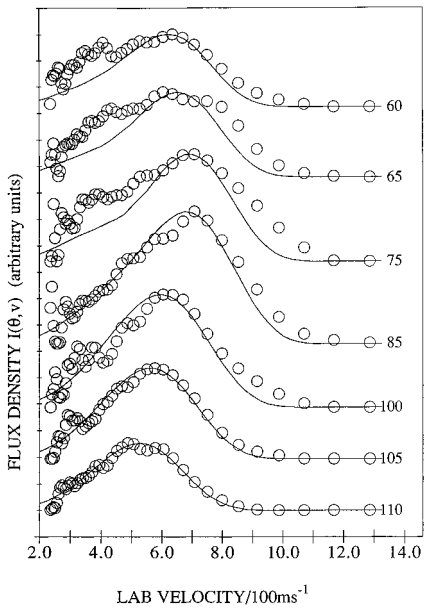

Figure 4. Laboratory velocity distributions (flux density) of reactively scattered IO from O + C_3H_5I at an initial translational energy $E \sim 16$ kJ mol^{-1}.

of IO from Radlein *et al.*[11] and C_3H_5I from Traeger[12] and the IO($^2\Pi_{1/2}$) excitation energy from Huber and Herzberg.[13] Contour maps of the center-of-mass differential cross section in Figure 7 illustrate the predominance of IO backward scattering at both initial translational energies.

No evidence was found for the formation of HOI reaction product, as was observed[1,2] in the reactions of O(^{3}P) atoms with C_2H_5I, $(CH_3)_2CHI$, and $(CH_3)_3CI$ molecules. No reactive scattering which could be identified with the hypothetical displacement pathway

$$O(^3P) + C_3H_5I \rightarrow C_3H_5O + I \qquad (3)$$

was detected in these experiments. Similarly, no BrO reaction product arising from the scattering of O(^{3}P) atoms with allyl

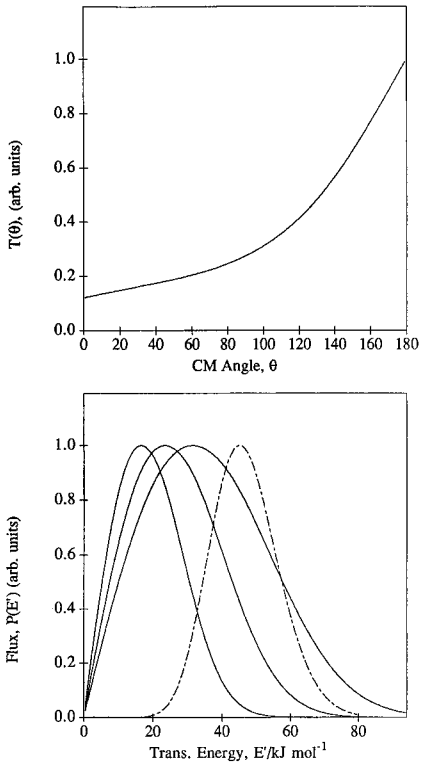

Figure 5. Angular function $T(\theta)$ and translational energy distributions $P(E')$ for IO products from O + C_3H_5I at initial translational energy E ~ 46 kJ mol^{-1}. Rightmost product translational energy distribution corresponds to $\theta = 180°$, center distribution to $\theta = 90°$, and leftmost distribution to $\theta = 0°$. Dashed energy curve shows the distribution of initial translational energy. The uncertainty in the relative intensity of forward scattering in the angular distribution is ~0.05 while the uncertainties in the peaks of product translational energy distributions are ~4 kJ mol^{-1}.

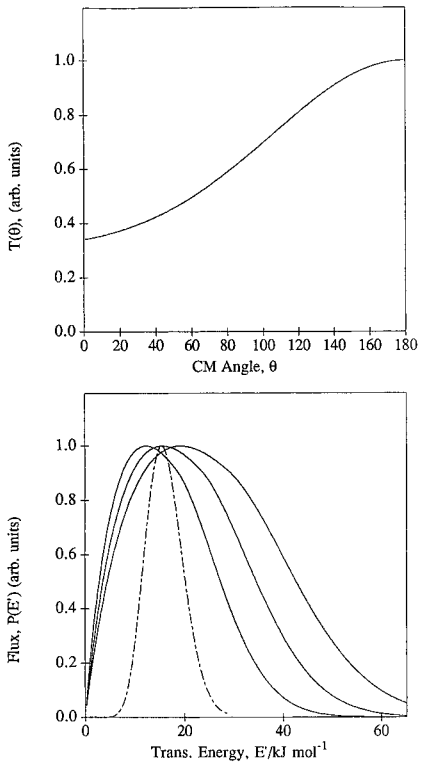

Figure 6. Angular functions $T(\theta)$ and translational energy distributions $P(E')$ for IO products from O + C_3H_5I at initial translational energy E ~ 16 kJ mol^{-1}. The uncertainties are the same as for Figure 5.

TABLE 2: Reaction Energetics (kJ mol^{-1}), Initial Translational Energy E, Peak Product Translational Energy E'_{pk}, Average Product Translational Energy E'_{av}, and Reaction Exoergicity ΔD_0

	E'_{pk}			E'_{av}			
E	0°	90°	180°	0°	90°	180°	ΔD_0
16	12	15	19	17	21	26	50 ± 10 (eq 1a)
46	17	23	31	19	27	37	22 ± 10 (eq 1b)

bromide molecules was detected in experiments on the reaction

$$O(^3P) + C_3H_5Br \rightarrow BrO + C_3H_5 \qquad (4)$$

Discussion

Recent studies[1,2] of the reactions of O(^{3}P) atoms with alkyl iodide molecules have shown evidence for intersystem crossing from the initial triplet potential energy surface to the underlying singlet potential energy surface which supports a stable OIR intermediate[14,15] that is predicted by valence shell electron pair repulsion theory[16] to be strongly bent. Potential energy profiles showing the analogous situation for O + C_3H_5I in Figure 8 exhibit a greater reaction exoergicity, which depletes the stability of the singlet OIC_3H_5 intermediate. The *ab initio* calculations of Marshall[17] predict a well depth of ~155 kJ mol^{-1} for $OICH_3$, and this value has also been used in estimating the well depth E_0 ~ 100 kJ mol^{-1} for OIC_3H_5 in Figure 8. The triplet potential energy surface has $^3\Pi$ symmetry about the OIC bonds in the collinear configuration. The correlation diagram of Figure 9 shows the $^3\Pi_1$ and $^3\Pi_2$ spin multiplet states correlating directly with ground state IO($^2\Pi_{3/2}$) reaction product, while the $^3\Pi_{0^+}$ and $^3\Pi_{0^-}$ spin multiplet states correlate with the electronically excited IO($^2\Pi_{1/2}$) reaction product. The singlet $^1\Sigma^+_{0^+}$ state is assumed to lie above the $^3\Pi$ states but below the $^3\Sigma^-$ states in the collinear OIC configuration. The $^3\Pi$ surface splits into a lower ^{3}A″ and a higher ^{3}A′ potential energy surface under Renner−Teller interaction[18] in bent OIC configurations. The singlet potential energy surface has ^{1}A′ symmetry in bent OIC configurations and again correlates with electronically excited O(^{1}D) reactant atoms but now correlates with ground state IO($^2\Pi_{3/2}$) reaction products as shown in Figure 8. The Renner−Teller state of ^{3}A″ symmetry also correlates with ground state IO($^2\Pi_{3/2}$) products as shown in Figure 8, while the Renner−Teller state of ^{3}A′ symmetry correlates with electronically excited IO($^2\Pi_{1/2}$) products.

In bent OIC configurations the *ab initio* calculations of Marshall[17] confirm that the singlet ^{1}A′ potential energy surface becomes the lowest surface and intersects the triplet ^{3}A″ potential energy surface in the entrance valley as shown in Figure 8. In the situation shown in Figure 9, the $^1\Sigma^+$ surface does not intersect the $^3\Pi$ surface so that intersystem crossing to the singlet state would not occur in the collinear configuration. However, in bent OIC configurations the ^{3}A″ states correlating with the $^3\Pi_2$ and $^3\Pi_{0^+}$ spin multiplet states in the collinear configuration each transform into an a′ spin multiplet state,[1,18] which couples to the ^{1}A′ state as shown in Figure 8, inducing intersystem crossing. However, the ^{3}A″ state correlating with the $^3\Pi_1$ spin multiplet state transforms into an a″ spin multiplet state[1,18] and is uncoupled to the ^{1}A′ state in Figure 8. For an angular correlation diagram showing this situation, see Figure 11 of ref 1. Consequently, direct reaction over the triplet potential energy surface is expected to be the preferred adiabatic process in near-collinear OIC configurations, but intersystem crossing in the entrance valley of the triplet potential energy surface is expected to become a competing process at the seam of intersection with the singlet surface in more strongly bent OIC configurations.

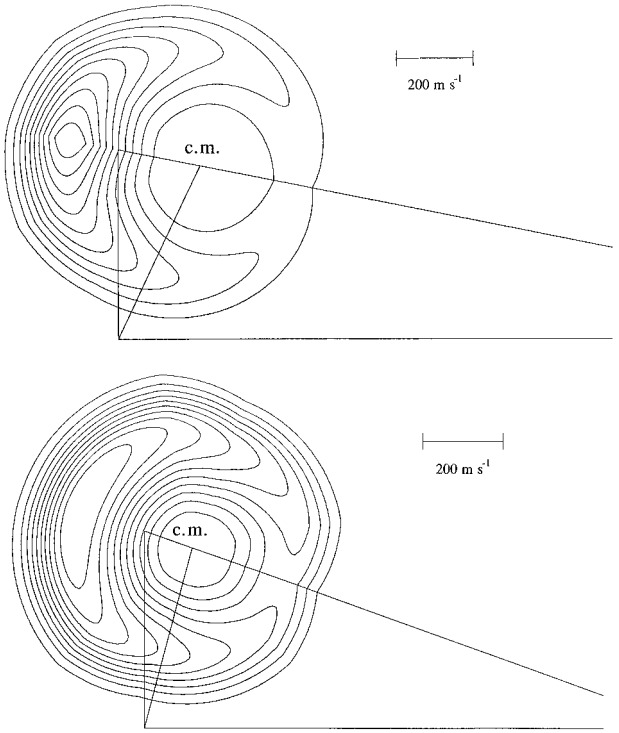

Figure 7. Contour maps of the differential cross section for IO scattering superimposed on the nominal Newton diagrams at $E \sim 46$ kJ mol^{-1} (upper panel) and $E \sim 16$ kJ mol^{-1} (lower panel).

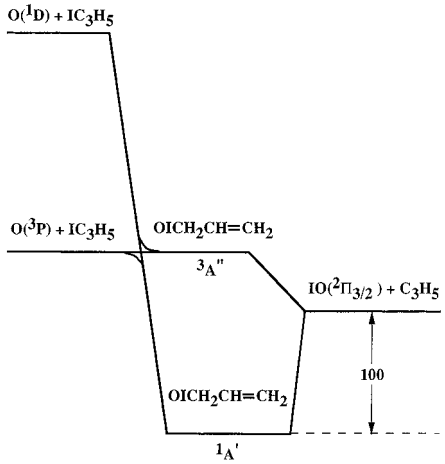

Figure 8. Potential energy profiles for the O + C_3H_5I reaction in bent OIC_3H_5 configurations, showing the intersection of the lowest singlet and triplet potential energy surfaces. Symbols refer to electronic symmetry about the OIC bonds. The well depth of the singlet OIC_3H_5 complex is estimated to be $E_0 = 100 \pm 20$ kJ mol^{-1} with respect to products.

The O + C_2H_5I reaction[1] at low initial translational energy $E \sim 16$ kJ mol^{-1} shows only scattering arising from a long-lived singlet OIC_2H_5 complex, while the backward scattered IO product attributed to direct reaction over the triplet potential energy surface emerges at higher initial translational energy. This was attributed to the presence of a barrier on the $^3A''$ potential energy surface. In contrast, the strongly backward scattered IO product for O + C_3H_5I in Figure 6 indicates that direct reaction over the triplet potential energy surface occurs at low initial translational energy $E \sim 16$ kJ mol^{-1}. Consequently, the $^3A''$ potential energy surface for O + C_3H_5I in Figure 8 is shown without any potential energy barrier. The product translational energy distributions in Figures 5 and 6 show the high translational energies for IO scattering in the backward direction which are associated with direct scattering

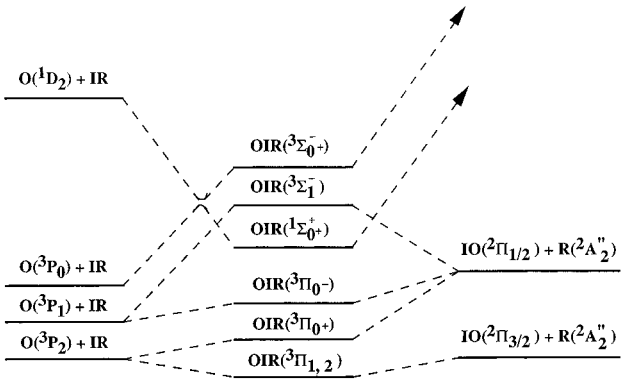

Figure 9. Correlation diagram for spin multiplet states for O atoms reacting with alkyl and allyl iodide molecules in the collinear OIC configuration with symbols referring to electronic symmetry about the OIC bonds. The IC bond is assumed to be of σ symmetry and the electronic state $^2A''_2$ is appropriate to the ground state of the alkyl radical R = CH_3.

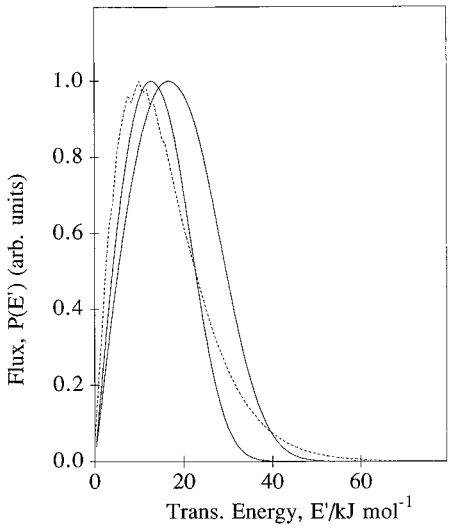

Figure 10. Product translational energy distribution calculated from phase space theory (broken curve) compared with the experimental distributions (solid curves) for IO forward scattering from O + C_3H_5I at initial translational energy $E \sim 46$ kJ mol^{-1}. The uncertainty in the product translational energy of the experimental distribution is estimated by showing upper and lower limits to the distribution for forward scattering.

over the triplet potential energy surface but significantly lower translational energies for IO scattering in the forward direction which may be associated with longer collision lifetimes of the singlet OIC_3H_5 intermediate. In the limit of a long-lived OIC_3H_5 complex dissociating without any intervening potential energy barrier, the product translational energy distributions should be well described by phase space theory.[19−21] The phase space product translational energy distributions calculated with initial maximum impact parameters $b_m = 2.5$ Å and $b_m = 3.1$ Å for O + C_3H_5I at initial translational energies $E \sim 46$ and 16 kJ mol^{-1} and final maximum impact parameter $b'_m = 2.5$ Å in Figures 10 and 11 predict equal or slightly lower translational energies than those observed for the forward scattering. This contrasts with the reactions of O atoms with ethyl iodide molecules[1] where the full range of IO product scattering at low inital translational energy is in agreement with the predictions of phase space theory.

Integration over the differential cross section for IO scattering

$$Q = 2\pi \int_0^{u_{max}} \int_0^{\pi} I_{cm}(\theta,u) \sin\theta \, d\theta \, du \qquad (5)$$

allowed the separate contributions of direct scattering over the

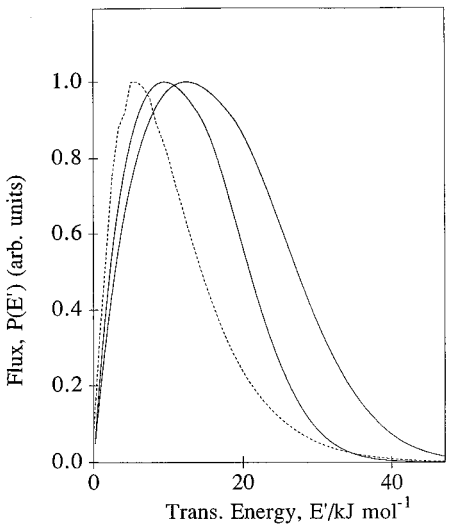

Figure 11. Product translational energy distribution calculated from phase space theory (broken curve) compared with the experimental distributions (solid curves) for IO forward scattering from O + C_3H_5I at initial translational energy $E \sim 16$ kJ mol^{-1}. The uncertainty in the product translational energy of the experimental distribution is estimated by showing upper and lower limits to the distribution for forward scattering.

triplet potential energy surface and dissociation of the long-lived OIR complex on the singlet potential energy surface to the total reaction cross section to be estimated[2] for the alkyl iodide reactions with R = C_2H_5, $(CH_3)_2CH$, and $(CH_3)_3C$. When the yield of HOI product was also taken into account, it was found that only a $\sim^1/_5$ of the total reaction cross section arose from direct reaction over the triplet potential energy surface at an initial translational energy $E \sim 51$ kJ mol^{-1}, while $\sim^4/_5$ arose from intersystem crossing to the singlet potential energy surface. When an analogous calculation is carried out for the differential cross section for IO scattering from O + C_3H_5I at an initial translational energy $E \sim 46$ kJ mol^{-1} in Figure 5, then it is found that the contribution from direct scattering over the triplet surface attributed to backward peaked scattering exceeds the contribution from the OIC_3H_5 intermediate on the singlet surface attributed to the isotropic scattering by a factor of ~2.5. This ratio must be regarded as only a rough estimate since in the absence of any HOI scattering, there is no independent indication of the angular distribution for the IO scattering via the singlet surface. The analogous calculation for the differential cross section of Figure 6 at an initial translational energy $E \sim 16$ kJ mol^{-1} shows backward and isotropic scattering making comparable contributions to the total reaction cross section.

The greater propensity for direct reaction over the triplet potential energy surface exhibited by allyl iodide compared with the alkyl iodide reactions may arise from reaction in near-collinear OIC configurations over the ^{3}A″ potential energy surface, which does not support a potential energy barrier and declines rapidly in the exit valley. Under these circumstances a reactive trajectory traverses the seam of intersection with the singlet surface in the entrance valley of the triplet potential energy surface at most once. However, the potential energy barrier in the entrance valley of the triplet surface for the alkyl iodide molecules results in frustrated trajectories which are impeded from direct reaction and may involve repeated traversals of the seam of intersection which can accumulate a high probability of intersystem crossing to the underlying singlet potential energy surface. Spin−orbit interaction is expected to be weak characteristic of the O(^{3}P) atom in the entrance valley of the potential energy surface with extended O−IC_3H_5 configurations but to become stronger in extended bent OI−C_3H_5 configurations. Consequently, frustrated trajectories which induce bending mode excitation in configurations with a contracted OI bond and an extended I−C bond will encounter stronger spin−orbit interaction on subsequent traversals of the seam of intersection.

The rebound scattering of IO product which is observed for direct reaction over the triplet potential energy surface indicates that reaction is confined to small impact parameter collisions $b_m \sim 2.5$ Å. The long-range form of the entrance valley of the ^{3}A″ potential energy surface may be judged from the van der Waals interaction of O(^{3}P) atoms with Xe atoms. Molecular beam measurements[22] of the total elastic scattering cross section indicate a very shallow potential energy well of depth $\epsilon = 1.7$ kJ mol^{-1} at a large internuclear distance $r_m = 3.7$ Å. Indeed, the broadening of the backward peak of IO scattering at lower initial translational energy in Figure 6,which reflects an increase in the maximum impact parameter for reaction, and the comparison with phase space calculations in Figure 11 suggest that reaction over the triplet surface may contribute to the IO scattering over the full range of center-of-mass angles. Likewise, the depleted binding energy of the singlet OIC_3H_5 intermediate may result in a lifetime comparable to its rotational period at higher initial translational energy and contribute to the angular distribution in Figure 5, favoring the backward direction for small impact parameter collisions.[23−25] Indeed, the ratio of the lifetime τ to the rotational period τ_{rot} may be estimated for the singlet OIC_3H_5 intermediate from the RRKM formula[26]

$$\frac{\tau}{\tau_{rot}} \approx \frac{L_m}{2\pi I_2^* \nu}\left(\frac{E + \Delta D_0 + E_0}{E + \Delta D_0}\right)^{s-1} \qquad (6)$$

which yields $\tau \sim 1.5\tau_{rot}$ for $E = 46$ kJ mol^{-1}, when using a maximum initial orbital angular momentum $L_m = 150\ \hbar$, a moment of inertia $I^*_2 = 1.1 \times 10^{-44}$ kg m^2, a mean vibrational frequency $\nu = 1.1 \times 10^{13}$ s^{-1}, and an effective number of vibrational modes $s = 7$. A short lifetime for the OIC_3H_5 complex may explain the discrepancies between the product translational energy for forward scattering and the predictions of phase space theory in Figures 10 and 11.

The absence of any HOI scattering in these experiments arises from the lack of a terminal CH_3 group[5] capable of forming a five-membered ring transition state. Abstraction from the CH group involves a strained bent configuration of the C_3H_5 compared with the collinear configuration of the allene product molecule.

$$O(^3P) + C_3H_5I \rightarrow HOI + C_3H_4 \qquad (7)$$

The absence of any detectable scattering according to the displacement pathway of eq 3 which would arise from O atom addition to the C═C double bond of the allyl radical also indicates that rearrangement of the singlet OIC_3H_5 complex to the alternative IOC_3H_5 isomer is inhibited by a potential energy barrier. The failure to observe BrO product from the scattering of O(^{3}P) atoms with allyl bromide molecules despite reaction according to eq 4 being thermoneutral with $\Delta D_0 = 6 \pm 5$ kJ mol^{-1} indicates the presence of a significant barrier on the triplet potential energy surface. This arises from the Br atom occupying the central location rather than the more electropositive I atom and renders the seam of intersection with the singlet potential energy surface inaccessible to collisions of O(^{3}P) atoms with hydrocarbon bromide molecules[2] under the conditions of these experiments.

Acknowledgment. Support of this work by EPSRC and the European Commission is gratefully acknowledged.

References and Notes

(1) Wang, J. J.; Smith, D. J.; Grice, R. *J. Phys. Chem.* **1996**, *100*, 6620.
(2) Wang, J. J.; Smith, D. J.; Grice, R. *J. Phys. Chem.* **1996**, *100*, 13603.
(3) Klaassen, J. J.; Lindner, J.; Leone, S. R. *J. Chem. Phys.* **1996**, *104*, 7403.
(4) Monks, P. S.; Stief, L. J.; Tardy, D. C.; Liebman, J. F.; Zhang, Z.; Kuo, S. C.; Klemm, R. B. *J. Phys. Chem.* **1995**, *99*, 16566.
(5) Gilles, M. K.; Turnipseed, A. A.; Talukdar, R. K.; Rudich, Y.; Villalta, P. W.; Huey, L. G.; Burkholder, J. B.; Ravishankara, A. R. *J. Phys. Chem.* , **1996**, *100*, 14005.
(6) White, R. W. P.; Smith, D. J.; Grice, R. *Chem. Phys. Lett.* **1992**, *193*, 269.
(7) Gorry, P. A.; Grice, R. *J. Phys. E* **1979**, *12*, 857.
(8) Nowikow, C. V.; Grice, R. *J. Phys. E* **1979**, *12*, 515.
(9) Entemann, E. A.; Herschbach, D. R. *Discuss. Faraday Soc.* **1967**, *44*, 289.
(10) Halpern, I.; Strutinski, V. M. *Proc. 2nd Intl. Conf. Peaceful Uses of Atomic Energy (Geneva)* **1958,** 408.
(11) Radlein, D. St. A. G.; Whitehead, J. C.; Grice, R. *Nature (London)* **1975**, *253*, 37.
(12) Traeger, J. C. *Int. J. Mass Spectrom. Ion Processes* **1984**, *58*, 259.
(13) Huber, K. P.; Herzberg, G. *Constants for Diatomic Molecules*; Van Nostrand Reinhold: New York, 1979.
(14) Clark, R. J. H.; Dunn, J. R. *J. Phys. Chem.* **1996**, *100*, 532.
(15) Hawkins, M.; Andrews, L. *Inorg. Chem.* **1984**, *24*, 3285.
(16) Gillespie, R. J. *Molecular Geometry*;Van Nostrand Reinhold: New York, 1969.
(17) Marshall, P. Private communication.
(18) Herzberg, G. *Electronic Spectra of Polyatomic Molecules*; Van Nostrand Reinhold: New York, 1966.
(19) Pechukas, P.; Light, J. C.; Rankin, C. *J. Chem. Phys.* **1966**, *44*, 794.
(20) Lin, J.; Light, J. C. *J. Chem. Phys.* **1966**, *45*, 2545.
(21) Light, J. C. *Discuss. Faraday Soc.* **1967**, *44*, 14.
(22) Aquilanti, V.; Candori, R.; Pirani, F. *J. Chem. Phys.* **1988**, *89*, 6157.
(23) Keane, N. W.; Smith, D. J.; Grice, R. *Laser Chem.* **1988**, *9*, 277.
(24) Brouard, M.; Lambert, H. M.; Russell, C. L.; Short, J.; Simons, J. P. *J. Chem. Soc., Faraday Discuss.* **1995**, *102*, 179.
(25) Grice, R. *J. Chem. Soc., Faraday Discuss.* **1995**, *102*, 255.
(26) White, R. W. P.; Smith, D. J.; Grice, R. *J. Phys. Chem.* **1993**, *97*, 2123.